Open access • Journal Article • DOI:10.1115/1.4026169

Comparisons of Radiative Heat Transfer Calculations in a Jet Diffusion Flame Using Spherical Harmonics and k-Distributions — Source link

Jian Cai, Ricardo Marquez, Michael F. Modest

Institutions: University of California, Merced

Published on: 01 Nov 2014 - Journal of Heat Transfer-transactions of The Asme (American Society of Mechanical Engineers)

Topics: Radiative transfer, Atmospheric radiative transfer codes, Spherical harmonics and Diffusion flame

Title

Comparisons of Radiative Heat Transfer Calculations in a Jet Diffusion Flame Using Spherical Harmonics and k-Distributions

Journal

JOURNAL OF HEAT TRANSFER-TRANSACTIONS OF THE ASME, 136(11)

ISSN

0022-1481

Authors

Cai, Jian
Marquez, Ricardo
Modest, Michael F

Publication Date

2014-11-01

DOI

10.1115/1.4026169

Peer reviewed

Jian Cai
School of Engineering,
University of California,
Merced, CA 95343
e-mail: jcai@ucmerced.edu

Ricardo Marquez
School of Engineering,
University of California,
Merced, CA 95343
e-mail: rmarquez3@ucmerced.edu

Michael F. Modest
Professor
Fellow ASME
School of Engineering,
University of California,
Merced, CA 95343
e-mail: mmodest@ucmerced.edu

Comparisons of Radiative Heat Transfer Calculations in a Jet Diffusion Flame Using Spherical Harmonics and *k*-Distributions

A new nongray radiation modeling library for combustion gases has been implemented in OpenFOAM. The spectral models for single species include gray, correlation tables and full spectrum k-distributions (FSK) assembled from a narrow-band database. Mixing models for k-distributions include the multiplication and uncorrelated mixture models. Radiative transfer equation solvers for the library include spherical harmonics such as P_1, P_3, SP_3 and SP_5 as well as the optically thin approximation. The performance of the different solution methods is compared for accuracy and speed as a tool for future model strategy selection. [DOI: 10.1115/1.4026169]

Keywords: radiative heat transfer, combustion, k-distribution methods, spherical harmonics

1 Introduction

Thermal radiation plays an important role in combustion systems. A high-fidelity radiation model that may be required to achieve accurate numerical predictions of the overall heat transfer in such systems requires both a radiative transfer equation (RTE) solver and a spectral model.

Although the radiative transfer equation (RTE), which includes emission, absorption and scattering of the participating medium, gives a complete description of radiative heat transfer, very few RTEs can be solved exactly because of their high dimensionality. Several competing approximate solution methods are available, such as the spherical harmonics method, the discrete ordinates method and the photon Monte Carlo method [1]. The discrete ordinates method (DOM) is very popular because of its ease of implementation and extension to high orders. However, because of large computational cost, only low-order calculations are generally carried out. Furthermore, this method suffers from ray effects, especially for low orders.

The spherical harmonics method is difficult to extend to high orders due to the complicated mathematics involved. However, the lowest order implementation, the P_1 method, and simplified higher order implementations are capable to provide respectable accuracy at very low computational cost. In the P_1 approximation, the RTE is converted into an elliptical PDE, which can be easily implemented within most CFD solvers. Because of its low order of truncation, the P_1 method tends to be more accurate in media with smooth directional variation of radiative intensity [1].

To overcome the mathematical complexity of the P_N approximation, the simplified P_N (SP_N) approximation was introduced as a three-dimensional extension to the one-dimensional slab P_N-formulation [2–4]. The resulting lower-order implementations, SP_3 and SP_5, are elliptic PDEs without cross-derivatives and contain fewer PDEs as compared to their P_N counterparts. The governing equations are similar to the simple P_1 equation, connected only through simple source terms.

The photon Monte Carlo (PMC), while computationally expensive, can readily be implemented for the most difficult radiative problems, such as strong spectral, spatial and directional variation of radiation properties. Its stochastic nature also makes it the only method capable of fully evaluating turbulence–radiation interaction (TRI) [5,6].

The solution of RTEs is further complicated by the spectral variations of radiative properties of participating media. Radiatively participating gases commonly involved in combustion include CO_2, H_2O and CO. Their absorption coefficients have strong spectral dependency. While the line-by-line (LBL) spectral model [7,8] provides the most accurate results for radiative heat transfer, its large computational demands prevent its use in practical engineering applications. Recently, full-spectrum *k*-distribution methods have been developed for gases [8–10]. A *k*-distribution is a spectrally reordered absorption coefficient over a narrow-band or the full spectrum. Using *k*-distributions, the radiative heat transfer can be determined with excellent accuracy, but at a small fraction of effort compared to LBL calculations. The full-spectrum *k*-distributions may be compiled from narrow-band *k*-distribution databases [11]. Alternatively, those of CO_2 or H_2O at atmospheric pressure may be evaluated using correlation tables. When more than one species is present, a mixing model is necessary to determine the *k*-distribution of the mixture from the *k*-distribution of each composition gas. Common mixing models include the multiplication model [12] and uncorrelated mixture model [10,1].

In this study, a nongray radiation library was implemented within OpenFOAM [13,14]. OpenFOAM is an open-source CFD package written in C++. It has a gray spectral model, P_1 and DOM RTE solvers. New spectral models implemented include the line-by-line model, *k*-distribution models and Planck-mean gray model. The RTE solvers include P_1, P_3, SP_3 and SP_5. Radiative heat sources using the mean scalar field of a turbulent flame are calculated using different model combinations for a sample combustion system. Comparisons are made in terms of accuracy and speed.

The novelty of this work is threefold: (1) to demonstrate the accuracy of the *k*-distribution models in a strongly nonhomogeneous practical flame, (2) to demonstrate the important coupling effects between RTE and nongray spectral models, in particular, the failure of the gray models for nongray gases, and (3) to introduce new RTE models (SP_3, SP_5, P_3) that can improve radiation calculations significantly with little additional cost.

Contributed by the Heat Transfer Division of ASME for publication in the Journal of Heat Transfer. Manuscript received August 14, 2013; final manuscript received November 26, 2013; published online September 16, 2014. Assoc. Editor: Zhixiong Guo.

2 Numerical Models

2.1 Spectral Models

2.1.1 Line-by-Line Models. The most accurate spectral model is the line-by-line (LBL) model, which follows all spectral variations with a fine spectral resolution. Required spectral resolution is usually less than 0.01 cm^{-1} for the spectral range from 50 cm^{-1} to 12000 cm^{-1}. This results in a million or so spectral points. A separate RTE evaluation is required on each spectral point. While line-by-line calculations provide the most accurate results, their computational cost prohibits them being used in practical simulations when coupled with a deterministic RTE solver. However, a line-by-line model can be coupled with a photon Monte Carlo solver with little additional cost [15].

2.1.2 Gray Model. The simplest spectral model is the gray model, which assumes no spectral variations. The spectral variables in the RTE are integrated beforehand, and the resulting RTE does not depend on a spectral variable. For nongray gases, the effective gray absorption coefficient is usually taken to be its Planck-mean value, because a gray calculation using the Planck mean absorption coefficient provides an exact evaluation of emission and thereby also the radiative heat source, if the absorption is negligible as in the optically thin limit.

2.1.3 Correlated Full-Spectrum k-Distributions. When self-absorption becomes important, nongray properties, which significantly affect the spectral intensity, have to be considered. While line-by-line calculations provide the most accurate results, k-distributions provide a cheap yet accurate alternative.

A k-distribution is a spectrally reordered absorption coefficient. In a full-spectrum k-distribution the absorption coefficient is weighted by the local Planck function for the calculation of cumulative k-distributions. When extending the k-distribution method to nonhomogeneous mixtures, the absorption coefficient is assumed to be correlated, i.e., if the absorption coefficient has the same value over a set of spectral locations at a certain thermodynamic state (known as the reference state), it has an identical (but different) value over the same set of spectral positions at other thermodynamic states [1,16].

If absorption coefficients are correlated between thermodynamic state $\boldsymbol{\phi}$ and the reference state $\boldsymbol{\phi}^0$, the same cumulative k distribution (g) value refers to the same spectral positions in both spectra. The absorption coefficient at this spectral position is determined by the k-distributions, namely, $k^*(g)$ for state $\boldsymbol{\phi}$ and $k(g)$ for the reference state $\boldsymbol{\phi}^0$. The variation of Planck functions due to the temperature difference between two states is accounted for by the ratio of the two k-distributions using the absorption coefficient evaluated at the reference state but weighted by Planck functions of two temperatures. The resulting ratio is the stretching factor a.

The reordering process changes the spectral variable from wavenumber to the cumulative k-distribution (g). Spectral totals are then determined by integration over g-space. For example, for incident radiation G, we have

$$G = \int_{\eta} G_{\eta} d\eta = \int_{0}^{1} G_g dg \tag{1}$$

The reordered absorption coefficients (k^*) is a monotonic function of g. Therefore, numerical integration over g may be carried out using Gaussian quadrature for high accuracy with very few spectral points (or RTE evaluations). As a result, instead of repeating radiative calculations over a million or so wavenumbers in a line-by-line calculation, a full-spectrum k-distribution calculation only requires radiation calculations for a few quadrature points. In this work all full-spectrum k-distribution calculations are performed using both 8 and 64 point quadratures to examine its sensitivity to quadrature schemes. It is found that the difference in predicting the radiative heat source, $-\nabla \cdot q$, between using 8 and 64 point quadratures is less than 3% for the here considered examples. This validates the use of few-point quadratures for full-spectrum k-distribution methods in nonhomogeneous media, and hence only the results from 8-point quadrature are reported here.

2.1.4 Narrow-Band Database. A narrow-band is a small spectral band over which the Planck function may be assumed

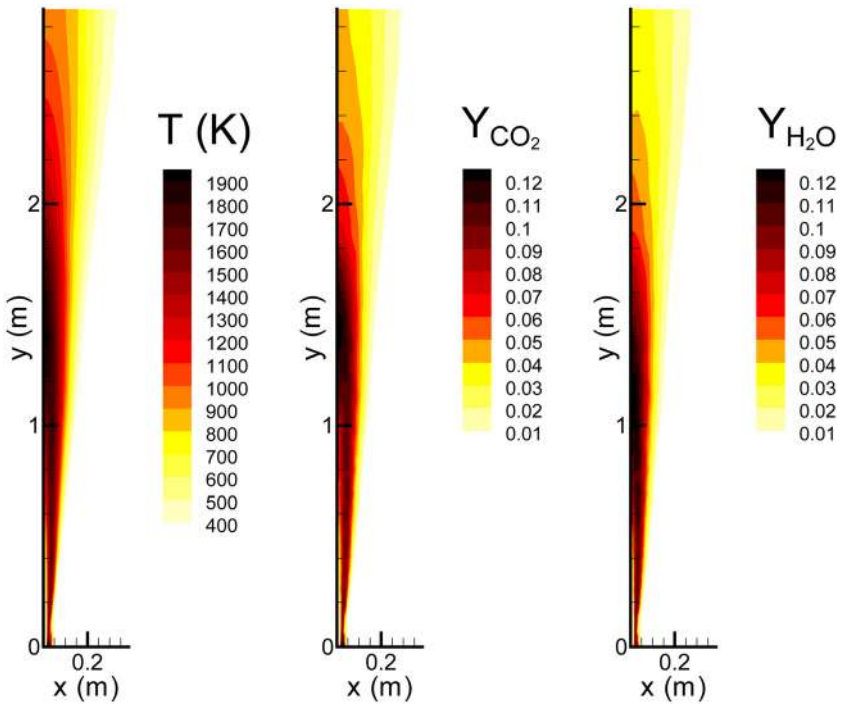

Fig. 1 Time-averaged spatial profile of temperature (left), CO_2 mass fraction (middle), and H_2O mass fraction (right) of enlarged Sandia Flame D

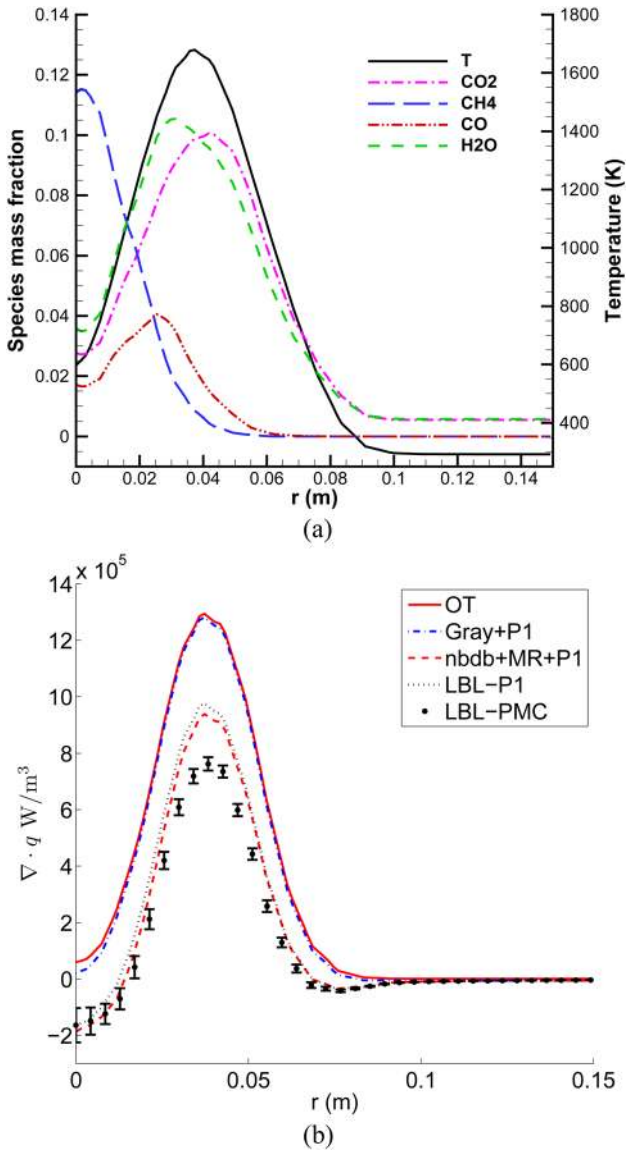

Fig. 2 Temperature and species mass fractions (*a*) and radiative heat flux divergence (*b*) at $y = 0.5$m. Legends abbreviations are "nbdb" for narrow-band database, "MR" for uncorrelated mixture (Modest–Riazzi) model, "lbl" for line-by-line spectral model, and "OT" for optically thin approximation.

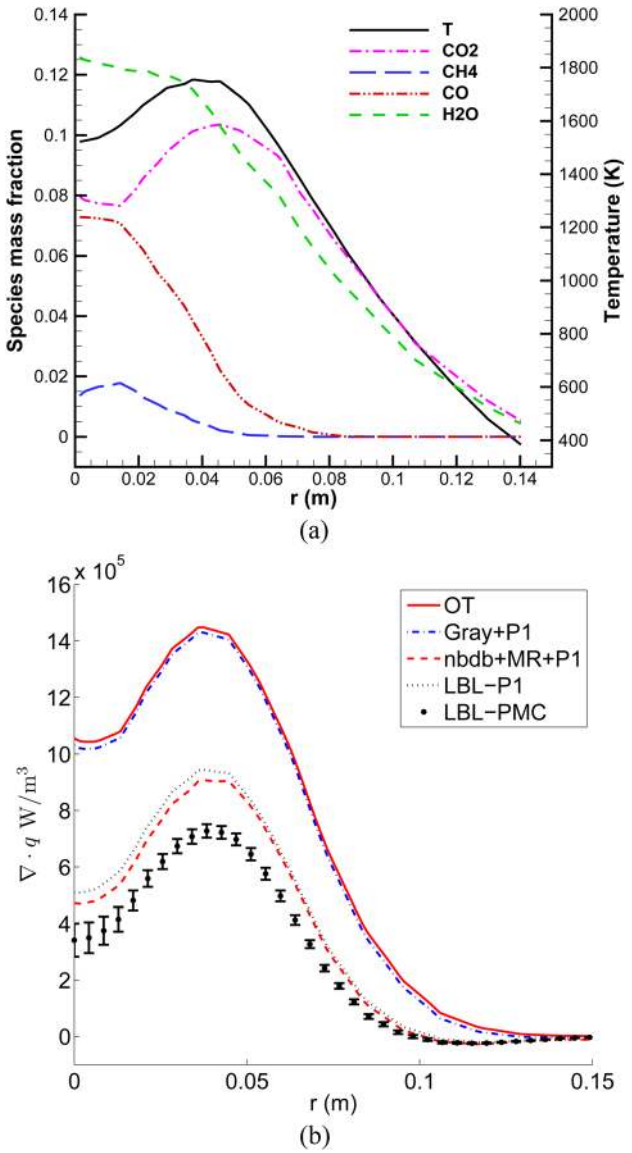

Fig. 3 Temperature and species mass fractions (*a*) and radiative heat flux divergence (*b*) at $y = 1.0$ m. Legend abbreviations are the same as Fig. 2.

constant. The k-distribution over a narrow-band is independent of the Planck function and can be databased [11,17]. The small spectral coverage also reduces the absorption coefficient variations and hence increases database accuracy. After interpolation between databased thermodynamics states for a narrow-band k-distribution at an arbitrary state, a full-spectrum k-distribution is assembled as a Planck function weighted sum of all narrow-band k-distributions [11]. The previous narrow-band database [11] has been updated here with the same data format using the recent HITEMP 2010 [18] for CO_2, H_2O, and CO, and HITRAN 2008 [19] for CH_4. HITEMP 2010 claims to be accurate up to 4000 K [18].

2.1.5 Correlation Tables. For common radiatively participating gases, such as CO_2 and H_2O, the full-spectrum k-distribution may be approximated from assumed profiles with coefficients determined from fitting the assumed profile to the true k-distributions. The resulting empirical formulae are called correlation tables. The correlation tables for CO_2 [20] and H_2O [21] provide computationally cheap evaluations of full-spectrum k-distributions, albeit at some loss of accuracy. Liu et al. recently updated the correlation tables for CO_2 and H_2O using the HITEMP-2010 spectroscopy database [22].

2.1.6 Mixing Models. As a result of the reordering process, the spectral position information is lost. To find the k-distribution of a mixture from the k-distribution of each component, two mixing models are frequently used, namely the multiplication [12] and the uncorrelated mixture [1,10] models.

The multiplication model assumes that absorption coefficients between different species are statistically independent variables and have the multiplication property as the probability of independent events. As a result the cumulative k-distribution of the mixture is related to the cumulative k-distribution of each species by [1]

$$g(k) = \prod_l g_l(k) \tag{2}$$

where $g_l(k)$ is the cumulative k-distribution of the lth species.

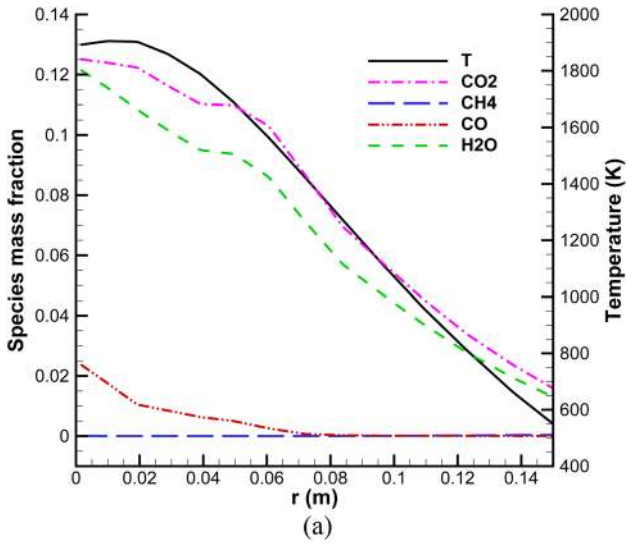

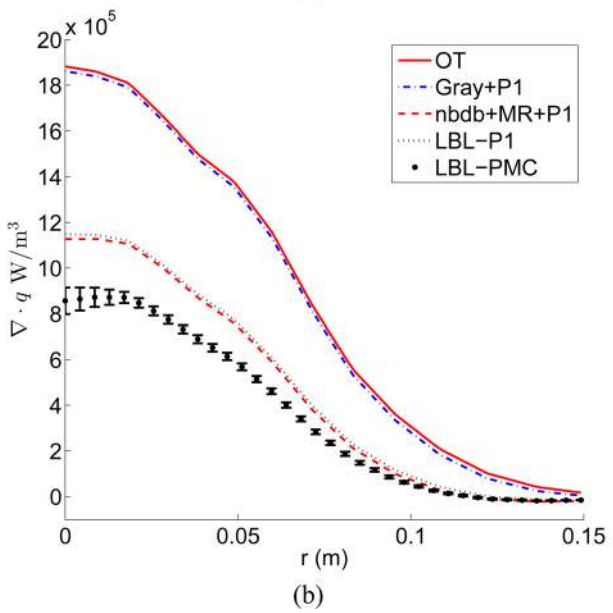

Fig. 4 Temperature and species mass fractions (*a*) and radiative heat flux divergence (*b*) at $y = 1.4$ m. Legend abbreviations are the same as Fig. 2.

Modest and Riazzi [10] recognized that the transmissivity over a narrow-band of a gas mixture to great accuracy is equal to the product of the transmissivity of each species, implying that the location of spectral lines of different species is uncorrelated. This implies that the Laplace transform of a k-distribution for a gas mixture is the product of each component gas, i.e.,

$$\mathcal{L}[f(k)] = \prod_l \mathcal{L}[f_l(k)] \tag{3}$$

For the case of two species, Eq. (3) leads to a convolution

$$g_{\text{mix}}(k_{\text{mix}}) = \int_0^1 g_2(k_{\text{mix}} - k_1(g_1))dg_1 \tag{4}$$

where $g_1(k_1), g_2(k_2)$ and $g_{\text{mix}}(k_{\text{mix}})$ are the cumulative k-distributions of the first, second species and mixture, respectively. The k-distribution of a mixture of more than two species can be evaluated using Eq. (4) recursively.

2.2 RTE Solvers

2.2.1 Optically Thin Approximation. The optically thin approximation neglects radiative self-absorption, and the radiative source term is simply the local emission (a sink) $-\nabla \cdot q = -4\kappa_P \sigma T^4$, and does not require a solution of the RTE. It gives the maximum radiative heat loss in a flame.

2.2.2 P_1 and P_3. In the P_1 method, the directional radiation intensity is approximated by spherical harmonics of the zeroth and first order. The resulting RTE is a Helmholtz type partial differential equation (PDE). For nonscattering media, the governing equation in the context of full-spectrum correlated k-distributions (FSCK) is

$$\frac{1}{k_g^*}\nabla \cdot \left(\frac{1}{3k_g^*}\nabla G_g\right) = 4\pi a_g I_{\text{b}} - G_g \tag{5}$$

where the subscript g denotes a "spectral" value from the cumulative k-distribution, G_g, k_g^* and a_g are incident radiation, correlated absorption coefficient and nongray stretching factor, respectively. Equation (5) is subject to the boundary condition

$$\frac{2-\epsilon}{\epsilon}\frac{2}{3k_g^*}\hat{\boldsymbol{n}} \cdot \nabla G_g + G_g = 4\pi a_{wg} I_{\text{bw}} \tag{6}$$

where ϵ is the wall emittance, $\hat{\boldsymbol{n}}$ the wall-normal direction unit vector pointing from medium to wall, and I_{bw} is the blackbody emission of the wall.

The P_3 method is a higher order counter-part to the P_1 method [23,24]. The PDEs for P_3 formulated for isotropic scattering [25] consist of six elliptical partial differential equations, which contain several terms with mixed partial derivatives. These PDEs and the associated Marshak boundary condition couple six intensity coefficients. A thorough description of the implementation details of the P_3 equations is provided in Refs. [25,26].

2.2.3 SP_3 and SP_5. The simplified P_5 (SP_5) equations for a FSCK implementation are [1,4]

$$\frac{1}{3k_g^*}\nabla \cdot \left(\frac{1}{k_g^*}\nabla J_{0g}\right) = J_{0g} - \frac{2}{3}J_{2g} + \frac{8}{15}J_{4g} - a_g I_{\text{b}} \tag{7a}$$

$$\frac{3}{7k_g^*}\nabla \cdot \left(\frac{1}{k_g^*}\nabla J_{2g}\right) = -2(J_{0g} - a_g I_{\text{b}}) + 3J_{2g} - \frac{12}{5}J_{4g} \tag{7b}$$

$$\frac{5}{11k_g^*}\nabla \cdot \left(\frac{1}{k_g^*}\nabla J_{4g}\right) = \frac{8}{3}(J_{0g} - a_g I_{\text{b}}) - 4J_{2g} + 5J_{4g} \tag{7c}$$

where the subscript g again denotes the cumulative k-distribution, k_g^* and a_g are the correlated absorption coefficient and the stretching factor, respectively. J_{0g}, J_{2g}, and J_{4g} are related to the coefficients of the three isotropic spherical harmonics. These three elliptic partial differential equations are subject to the following boundary conditions, respectively,

$$-\frac{1}{3k_g^*}\hat{\boldsymbol{n}} \cdot \nabla J_{0g} = \frac{1}{2}(J_{0g} - J_w/\pi) - \frac{1}{8}J_{2g} + \frac{1}{16}J_{4g} \tag{8a}$$

$$-\frac{1}{7k_g^*}\hat{\boldsymbol{n}} \cdot \nabla J_{2g} = -\frac{1}{8}(J_{0g} - J_w/\pi) + \frac{7}{24}J_{2g} - \frac{41}{384}J_{4g} \tag{8b}$$

$$-\frac{1}{11k_g^*}\hat{\boldsymbol{n}} \cdot \nabla J_{4g} = \frac{1}{16}(J_{0g} - J_w/\pi) - \frac{41}{384}J_{2g} + \frac{407}{1920}J_{4g} \tag{8c}$$

where $J_w = \pi a_{wg} I_w$ is the radiosity at the wall [1]. The solution gives incident radiation as

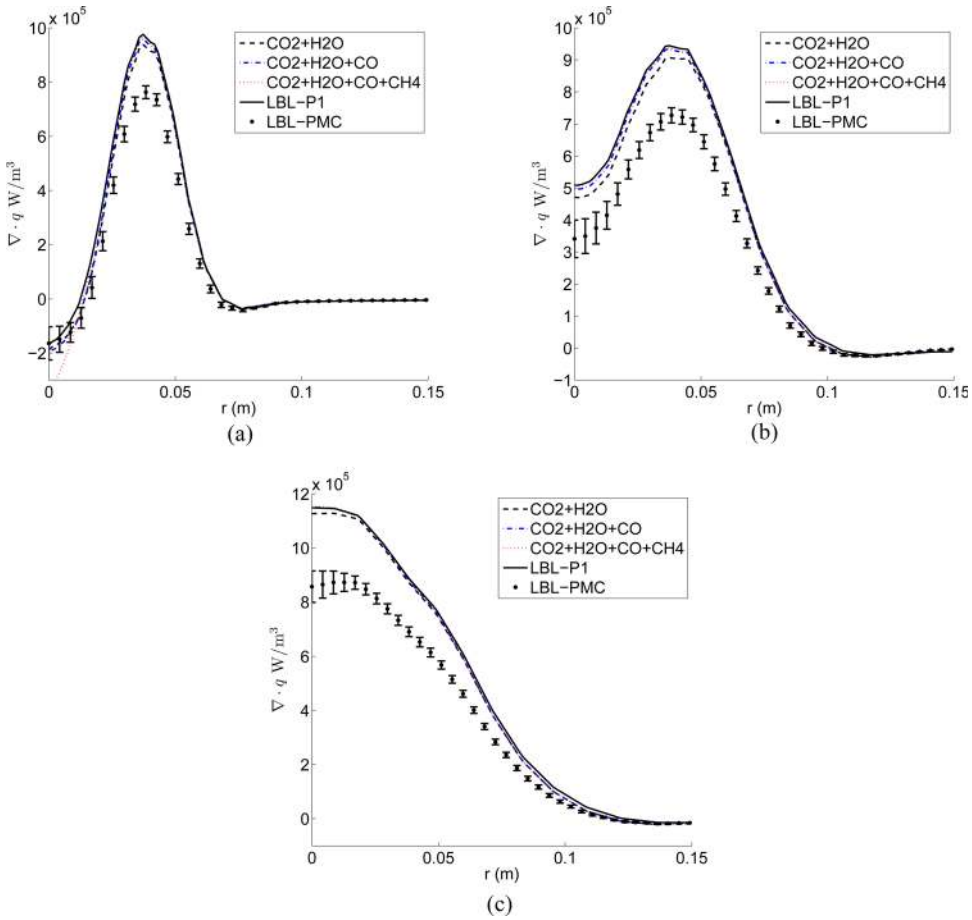

Fig. 5 Effects of species on radiative heat flux divergence $\nabla \cdot q$ at three downstream locations $y = 0.5$ m (*a*), $y = 1.0$ m (*b*), and $y = 1.4$ m (*c*)

$$G_g = 4\pi\left(J_{0g} - \frac{2}{3}J_{2g} + \frac{8}{15}J_{4g}\right) \tag{9}$$

The equations and boundary conditions for the simplified P_3 (SP_3) can be recovered from the above SP_5 equations and boundary conditions by forcing the highest component J_{4g} to be zero and deleting Eqs. (7*c*) and (8*c*).

2.3 Implementation. The *k*-distribution spectral models developed from previous research [10,11,17,20,21] were written in Fortran. They are connected to OpenFOAM using C-Fortran interoperation introduced in Fortran 2003 standard [27]. The RTE models (P_1, P_3, SP_3 and SP_5) are implemented using OpenFOAM built-in support on discretization of differential operators, such as ∇, ∇^2 [14]. Coupled equations in P_3, SP_3 and SP_5 RTE models are solved in sequence and iteratively until all equations are converged. When coupled with a *k*-distribution model, the RTEs are solved repeatedly for each quadrature based on the radiative properties at that quadrature. The spectral and RTE models are organized into two categories, so that any spectral model may be coupled with any RTE models easily. The nongray radiation module interfaces with OpenFOAM through the references to thermodynamic variables (temperature, pressure, and composition) and radiative heat sources.

2.4 Combustion Scalar Profiles. The flame investigated in this paper is a methane—air partially premixed flame derived from Sandia Flame D [28] by artificially quadrupling the jet diameter [29,6]. The velocity is reduced accordingly to retain the Reynolds number (Re = 22400). Sandia Flame D is a small laboratory-scale flame with correspondingly little radiation. Artificially increasing the size of the flame displays stronger radiation effects, such as are found in practical combustion configurations.

The flame was simulated in a two-dimensional axisymmetric mesh with full turbulence–radiation interaction [6]. Only the quasi-steady time-averaged temperature and species mass fraction fields (Fig. 1) are used here for radiation calculation comparisons. Hence, no turbulence–radiation interaction is considered, only the radiative heat flux divergence ($\nabla \cdot q$) is determined without feedback to the flame.

3 Results and Discussion

3.1 Effects of Nongray Absorption. The cross-sectional profiles of temperature and concentrations as well as local radiative heat source $\nabla \cdot q$ are plotted in Figs. 2–4, respectively, at three downstream locations. At downstream location $y = 0.5$ m, the flame is annular (Fig. 2), and the core shows significant unburned methane. The radiative flux divergence $\nabla \cdot q$, evaluated with different spectral models is compared at the bottom of Fig. 2. The optically thin approximation (OT) coupled with Planck-mean absorption coefficients gives the flame emission. Also shown are results from a photon Monte Carlo simulation coupled with a line-by-line spectral model (LBL-PMC), which gives the true radiative heat source [15]. The difference between the two lines is due to absorption. At this location approximately 40% of the emission is self-absorbed. If the gas is modeled as gray, the corresponding absorption calculated via the P_1 solver is negligible. This is because the Planck mean absorption coefficient used in the gray model is spectrally averaged, which significantly underestimates

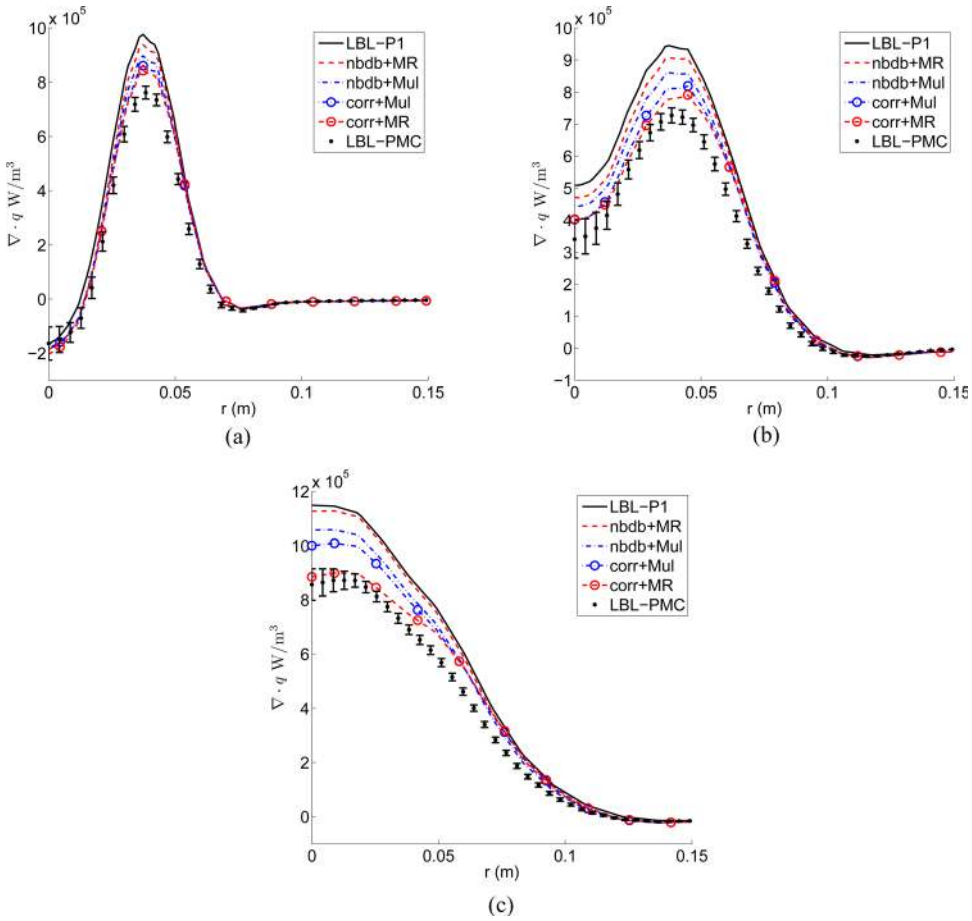

Fig. 6 Effects of mixing models on radiative heat flux divergence $\nabla \cdot q$ for different mixing models at three downstream locations $y = 0.5$ m (*a*), $y = 1.0$ m (*b*), and $y = 1.4$ m (*c*). LBL-P1 and LBL-PMC are also included for reference. Legend abbreviations are the same as Fig. 2.

gas absorption. When nongray effects are considered, P_1 coupled with the line-by-line spectral model recovers over 2/3 of the absorption. The remaining 1/3 is due to the P_1 approximation error. Also included in the comparison are the results of the P_1 coupled with the full-spectrum k-distributions. The full-spectrum k-distributions are assembled from the databased narrow-band k-distributions for CO_2 and H_2O and mixed using the uncorrelated mixture model at the narrow-band level. When coupled with the P_1 solver, the full-spectrum k-distribution (FSK) methods predict the $\nabla \cdot q$ close to that from the line-by-line model. This suggests the full-spectrum k-distributions achieve comparable accuracy to the line-by-line spectral model. Compared to little self absorption recovered by the gray model, results from the line-by-line and the full-spectrum k-distribution models suggest that for gas radiation with not-so-small optical thicknesses, a nongray spectral model is more important than the RTE solver because of gas spectral windows. Similar trends are also observed at $y = 1$ m in Fig. 3.

At $y = 1.4$ m (Fig. 4), approximately where the temperature peaks, all species other than CO_2 and H_2O have little concentration. Because of both high CO_2 and H_2O concentrations and temperature, the flame has its strongest emission. However, this does not lead to significant radiative heat loss as suggested by $\nabla \cdot q$, because highly concentrated CO_2 and H_2O absorb over a half of the emission. For all three locations, P_1 coupled with the full-spectrum k-distribution method gives a better prediction than gray models. The full-spectrum k-distribution models using the narrow-band database achieve close to LBL accuracy.

The gray Planck-mean absorption coefficients used in gray models fail to capture absorption in this calculation because of neglecting nongray effects. The nongray emission from participating gases is concentrated over wavenumbers with high absorption coefficients, where strong absorption occurs also. An averaged value, e.g., Planck-mean absorption coefficients, preserves emission but cannot capture (i.e., greatly underpredicts) nongray absorption.

3.2 Effects of Radiating Species. The differences in $\nabla \cdot q$ predictions between the narrow-band database and LBL calculations are further examined by the inclusion of different species, as shown in Fig. 5. The spectral model employed is a narrow-band k-distribution database coupled with the Modest–Riazzi mixing model at the narrow-band level. The RTE solver is P_1. LBL-PMC and line-by-line P_1 predictions are also included for comparison. For all three locations, considering 2 species (CO_2 and H_2O) gives close to line-by-line results with a maximum error of 7.5% occurred along the centerline ($r = 0$ m) at $y = 1.0$ (see Fig. 5) due to the omission of CO. Inclusion of CO shows that the three-species FSK returns essentially line-by-line accuracy, and that the contributions to emission from CH_4 is small. Adding CH_4 also results in an overprediction of absorption in the methane core at $y = 0.5$ m, because the FSK method relies on the assumption that the gases are correlated, which is challenged in nonhomogeneous combustion gas mixtures. In particular, in this flame, the methane absorption band does not overlap with emission bands of other species, and the correlation assumption gives false absorption.

3.3 Effects of *k*-Distribution and Mixing Models. The effects of k-distribution mixing models are demonstrated in Fig. 6. For k-distributions constructed from a narrow-band database the

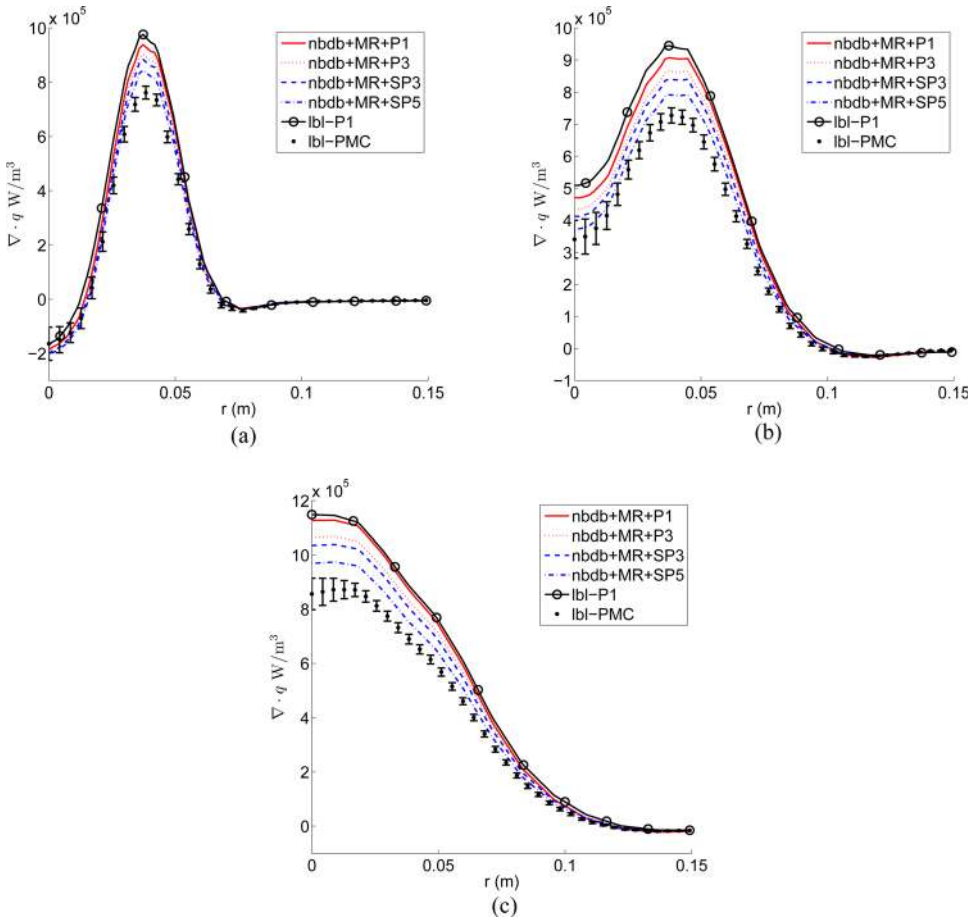

Fig. 7 Effects of RTE solvers on radiative heat flux divergence $\nabla \cdot q$ at three downstream locations $y = 0.5$ m (*a*), $y = 1.0$ m (*b*), and $y = 1.4$ m (*c*)

multiplication and uncorrelated mixture (Modest–Riazzi) mixing models are applied on each narrow-band before the resulting narrow-band k-distribution is compiled into its full-spectrum counterpart. For the correlation tables the mixing models are applied at the full spectrum level. Only the results using two species (CO_2 and H_2O) are shown for a fair comparison between the narrow-band database and the correlation tables. Mixing CO into the mixture FSK using the uncorrelated mixture model achieves line-by-line accuracy as shown in the previous section and Fig. 5.

For all three locations, the correlation tables underestimate $\nabla \cdot q$. This might be due to the fact that the correlation tables [20,21] are derived from the CDSD [30] and HITEMP-1995 [31] spectroscopic databases for CO_2 and H_2O, respectively, which include fewer spectral lines at high temperature than HITEMP 2010 [18] used for the present narrow-band database and LBL calculations.

The uncorrelated mixture model applied to the narrow-bands gives the least error for all three locations, while the multiplication model gives larger error. When mixing models are applied at the full-spectrum level, while using the correlation tables, the multiplication mixing model gives less error for the present conditions apparently due to compensating errors.

3.4 Effects of RTE Solvers. The $\nabla \cdot q$ calculations employing different RTE solvers are presented in Fig. 7. P_1, P_3, SP_3 and SP_5 RTE solvers are coupled with full-spectrum k-distributions assembled from a narrowband database and mixed with the uncorrelated mixture mixing model at the narrowband level. The trends when using different RTE solvers together with the correlation tables and the multiplication mixing model are identical to those using narrowband database generated full-spectrum k-distributions and therefore not included in the figures. When coupled with a k-distribution, SP_3 recovers over 30% of the difference between P_1 and PMC, while SP_5 recovers over one half. P_3 predictions are very close to SP_3. The simplified P_N methods require 2 or 3 elliptical equations, respectively, and therefore provide relatively cheap improvements over P_1 RTE evaluations. However, when coupled with the Planck-mean gray model, SP_3 and SP_5 (not shown) show little difference to P_1 predictions. This further confirms that the spectrally averaged Planck mean absorption coefficients significantly underestimate the gas absorption.

Table 1 Per cell and total time cost (in seconds) for a *k*-distribution evaluation of CO_2 and H_2O mixture

Per cell/total	Multiplication	Uncorrelated mixture
Correlation tables	0.0016/5.32	0.006/19.95
Narrow-band database	0.0549/182.5	0.469/1560

3.5 Computational Times. The time costs for k-distribution evaluations of the CO_2 and H_2O mixture per cell is shown in Table 1. The correlation tables require little cpu time. Evaluations using the narrow-band database require much more time because of database interpolation, mixing evaluation for each narrow-band, and assembly of narrow-band to full-spectrum k-distributions. The RTE models, P_1, P_3, SP_3 and SP_5 require 0.0312s, 2.95, 0.125 s and 0.172 s, respectively, for each quadrature on average, as compared in Table 2. Because SP_3 and SP_5 involve extra iterations between 2 and 3 equations, respectively, their time costs

Table 2 Per quadrature and total time cost (in seconds) for RTE solutions

	P_1	P_3	SP_3	SP_5
Per quadrature	0.0312	2.95	0.125	0.172
8 quadratures total	0.25	23.6	1.00	1.38

are, therefore, more than 2 and 3 times of the P_1 time cost, respectively.

The P_3 method consists of 4 simultaneous equations and, depending on coupling, should require 4 to 16 times the CPU requirements for P_1. However, the present implementation uses a straight OpenFOAM "additional equation" solution, which is very inefficient for simultaneous equations with cross-derivatives. No such problem is apparent for the SP_N equations (which have no cross-derivatives and which are only weakly coupled).

The present calculations are based on a mesh of 3325 cells and a 8 point quadrature scheme for the cumulative k-distribution. The total time for k-distribution assembly is 5.3 and 1560 s for correlation tables mixed with the multiplication model and narrow-band database mixed with uncorrelated mixture model, respectively, which represent computationally the cheapest and the most expensive k-distribution models in the present study. The total time for RTE solutions is 0.25, 23.6, 1.00 and 1.38 s for P_1, P_3, SP_3 and SP_5, respectively (Table 2). Since the total computational time is dominated by assembling k-distributions, simplified P_N methods provide relatively cheap improvements over P_1 methods.

4 Conclusions

The flame considered in this paper, with its enlarged optical thickness, shows significant self-absorption. Most of the emission and absorption is due to CO_2 and H_2O. The effect of absorption is essentially not captured at all by gray spectral models because gas absorption coefficients are banded. Using the k-distribution method, a nongray spectral model coupled with the simple P_1 RTE solver recovers about 2/3 of the absorption. Correlation tables provide a computationally cheap but less accurate evaluation of the k distributions. The narrow-band database coupled with the Modest–Riazzi mixing model achieves line-by-line accuracy. The multiplication model seems to predict lower radiative heat loss than the uncorrelated mixture model. However, the multiplication mixing model is computationally cheaper than the uncorrelated mixture model.

Simplified P_N models significantly improve the accuracy of radiation calculations over the P_1 model. Although simplified P_N models require iterations between equations, the additional computational time cost is small compared to that of assembling the k-distributions.

Acknowledgment

This research is sponsored partially by AFOSR under Grant No. FA9550-10-1-0148 and partially by NETL under Grant No. DE-FE0003801.

Nomenclature

a = nongray stretching factor
G = incident radiation ($W \cdot m^{-2}$)
g = cumulative k distribution
I_b = Planck function ($W \cdot m^{-2}$)
J = coefficient of isotropic spherical harmonics ($W \cdot m^{-2}$)
k = absorption coefficient variable (cm^{-1})
k^* = correlated reordered absorption coefficient (cm^{-1})
$\mathcal{L}$ = Laplace transform
$\hat{\boldsymbol{n}}$ = wall normal direction unit vector
q = radiative heat flux vector ($W \cdot m^{-2}$)
Re = Reynolds number
r = radial coordinate (m)
T = temperature (K)
y = axial coordinate (m)
η = wavenumber (cm^{-1})
ϵ = wall emittance
κ = absorption coefficient (cm^{-1})
κ_P = Planck-mean absorption coefficient (cm^{-1})
σ = Stefan-Boltzmann constant = $5.670 \times 10^{-8} W m^{-2} K^{-4}$
$\boldsymbol{\phi}$ = thermodynamic state vector
$\boldsymbol{\phi}^0$ = reference thermodynamic state vector

References

[1] Modest, M. F., 2013, *Radiative Heat Transfer*, 3rd ed., Academic Press, New York.
[2] Gelbard, E., 1961, "Simplified Spherical Harmonics Equations and Their Use in Shielding Problems," Atomic Power Laboratory, Technical Report No. WAPD-T-1182.
[3] McClarren, R. G., 2011, "Theoretical Aspects of the Simplified P_n Equations," Transp. Theory Stat. Phys., **39**(2–4), pp. 73–109.
[4] Modest, M. F., and Lei, S., 2012, "The Simplified Spherical Harmonics Method for Radiative Heat Transfer," Proceedings of Eurotherm Seminar 95, Elsevier, New York.
[5] Wang, A., and Modest, M. F., 2007, "An Adaptive Emission Model for Monte Carlo Ray-Tracing in Participating Media Represented by Statistical Particle Fields," J. Quant. Spectrosc. Radiat. Transf., **104**(2), pp. 288–296.
[6] Wang, A., Modest, M. F., Haworth, D. C., and Wang, L., 2008, "Monte Carlo Simulation of Radiative Heat Transfer and Turbulence Interactions in Methane/Air Jet Flames," J. Quant. Spectrosc. Radiat. Transf., **109**(2), pp. 269–279.
[7] Taine, J., 1983, "A Line-By-Line Calculation of Low-Resolution Radiative Properties of CO_2–CO–Transparent Nonisothermal Gases Mixtures up to 3000 K," J. Quant. Spectrosc. Radiat. Transf., **30**(4), pp. 371–379.
[8] Zhang, H., and Modest, M. F., 2002, "A Multi-Scale Full-Spectrum Correlated-k Distribution for Radiative Heat Transfer in Inhomogeneous Gas Mixtures," J. Quant. Spectrosc. Radiat. Transf., **73**(2–5), pp. 349–360.
[9] Wang, L., and Modest, M. F., 2005, "Narrow-Band Based Multi-Scale Full-Spectrum k-Distribution Method for Radiative Transfer in Inhomogeneous Gas Mixtures," ASME J. Heat Transfer, **127**, pp. 740–748.
[10] Modest, M. F., and Riazzi, R. J., 2005, "Assembly of Full-Spectrum k-Distributions From a Narrow-Band Database; Effects of Mixing Gases, Gases and Nongray Absorbing Particles, and Mixtures With Nongray Scatterers in Nongray Enclosures," J. Quant. Spectrosc. Radiat. Transf., **90**(2), pp. 169–189.
[11] Wang, A., and Modest, M. F., 2005, "High-Accuracy, Compact Database of Narrow-Band k-Distributions for Water Vapor and Carbon Dioxide," J. Quant. Spectrosc. Radiat. Transf., **93**, pp. 245–261.
[12] Solovjov, V. P., and Webb, B. W., 2000, "SLW Modeling of Radiative Transfer in Multicomponent Gas Mixtures," J. Quant. Spectrosc. Radiat. Transf., **65**, pp. 655–672.
[13] OpenFOAM website, http://www.openfoam.com/
[14] Weller, H., Tabor, G., Jasak, H., and Fureby, C., 1998, "A Tensorial Approach to Computational Continuum Mechanics Using Object-Oriented Techniques," Comput. Phys., **12**(6), pp. 620–631.
[15] Wang, A., and Modest, M. F., 2007, "Spectral Monte Carlo Models for Nongray Radiation Analyses in Inhomogeneous Participating Media," Int. J. Heat Mass Transfer, **50**, pp. 3877–3889.
[16] Modest, M. F., 2003, "Narrow-Band and Full-Spectrum k-Distributions for Radiative Heat Transfer—Correlated-k vs. Scaling Approximation," J. Quant. Spectrosc. Radiat. Transf., **76**(1), pp. 69–83.
[17] Pal, G., and Modest, M. F., 2010, "A Narrow-Band Based Multi-Scale Multi-Group Full-Spectrum k-Distribution Method for Radiative Transfer in Nonhomogeneous Gas–Soot Mixture," ASME J. Heat Transfer, **132**, pp. 023307–1–023307–9.
[18] Rothman, L. S., Gordon, I. E., Barber, R. J., Dothe, H., Gamache, R. R., Goldman, A., Perevalov, V. I., Tashkun, S. A., and Tennyson, J., 2010, "HITEMP, The High-Temperature Molecular Spectroscopic Database," J. Quant. Spectrosc. Radiat. Transf., **111**(15), pp. 2139–2150.
[19] Rothman, L. S., Gordon, I. E., Barbe, A., Benner, D. C., Bernath, P. F., Birk, M., Boudon, V., Brown, L. R., Campargue, A., Champion, J.-P., Chance, K., Coudert, L. H., Dana, V., Devi, V. M., Fally, S., Flaud, J.-M., Gamache, R. R., Goldman, A., Jacquemart, D., Kleiner, I., Lacome, N., Lafferty, W. J., Mandin, J.-Y., Massie, S. T., Mikhailenko, S. N., Miller, C. E., Moazzen-Ahmadi, N., Naumenko, O. V., Nikitin, A. V., Orphal, J., Perevalov, V. I., Perrin, A., Predoi-Cross, A., Rinsland, C. P., Rotger, M., Simeckova, M., Smith, M. A. H., Sung, K., Tashkun, S. A., Tennyson, J., Toth, R. A., Vandaele, A. C., and Auwera, J. V., 2009, "The HITRAN 2008 Molecular Spectroscopic Database," J. Quant. Spectrosc. Radiat. Transf., **110**(9–10), pp. 533–572.
[20] Modest, M. F., and Mehta, R. S., 2004, "Full Spectrum k-Distribution Correlations for CO_2 From the CDSD-1000 Spectroscopic Databank," Int. J. Heat Mass Transfer, **47**, pp. 2487–2491.
[21] Modest, M. F., and Singh, V., 2005, "Engineering Correlations for Full Spectrum k-Distribution of H_2O From the HITEMP Spectroscopic Databank," J. Quant. Spectrosc. Radiat. Transf., **93**, pp. 263–271.
[22] Liu, F., Chu, H., Zhou, H., and Smallwood, G., 2012, "Evaluation of the Absorption Line Blackbody Distribution Function of CO_2 and H_2O Using the

Proper Orthogonal Decomposition and Hyperbolic Correlations," J. Quant. Spectrosc. Radiat. Transf., **128**, pp 27–33.
[23] Yang, J., and Modest, M. F., 2007, "High-Order *P-N* Approximation for Radiative Transfer in Arbitrary Geometries," J. Quant. Spectrosc. Radiat. Transf., **104**(2), pp. 217–227.
[24] Modest, M. F., and Yang, J., 2008, "Elliptic PDE Formulation and Boundary Conditions of the Spherical Harmonics Method of Arbitrary Order for General Three-Dimensional Geometries," J. Quant. Spectrosc. Radiat. Transf., **109**, pp. 1641–1666.
[25] Modest, M. F., 2012, "Further Development of the Elliptic PDE Formulation of the P-N Approximation and Its Marshak Boundary Conditions," Numer. Heat Transfer, Part B, **62**(2–3), pp. 181–202.
[26] Marquez, R., and Modest, M. F., 2012, "Implementation of the Pn-Approximation for Radiative Heat Transfer on Openfoam," Proceedings of the ASME 2012 Summer Heat Transfer Conference, Paper No. HT2013-17556.
[27] Adams, J. C., Brainerd, W. S., Hendrickson, R. A., Maine, R. E., Martin, J. T., and Smith, B. T., 2009, *The Fortran 2003 Handbook*, Springer, New York.
[28] Barlow, R. S., and Frank, J. H., 1998, "Effects of Turbulence on Species Mass Fractions in Methane/Air Jet Flames," Proc. Combust. Inst., **27**, pp. 1087–1095.
[29] Li, G., and Modest, M. F., 2003, "Importance of Turbulence–Radiation Interactions in Turbulent Diffusion Jet Flames," ASME J. Heat Transfer, **125**, pp. 831–838.
[30] Tashkun, S. A., Perevalov, V. I., Teffo, J.-L., Bykov, A. D., and Lavrentieva, N. N., 2003, "CDSD-1000, The High-Temperature Carbon Dioxide Spectroscopic Databank," J. Quant. Spectrosc. Radiat. Transf., **82**(1–4), pp. 165–196.
[31] Rothman, L. S., Wattson, R. B., Gamache, R. R., Schroeder, J., and McCann, A., 1995, "HITRAN, HAWKS and HITEMP High Temperature Databases," Proc. SPIE, **2471**, pp. 105–111.